Addressing Electronic Effects in the Semi-Hydrogenation of Ethyne by $InPd_2$ and Intermetallic Ga-Pd Compounds

Yuan Luo[1], *Sebastián Alarcón Villaseca*[1], *Matthias Friedrich*[2], *Detre Teschner*[2], *Axel Knop-Gericke*[2], *Marc Armbrüster*[3,*]

[1] Max-Planck-Institut für Chemische Physik fester Stoffe, Nöthnitzer Str. 40, 01187 Dresden, Germany

[2] Department of Inorganic Chemistry, Fritz Haber Institute of the Max Planck Society, Faradayweg 4-6, 14195 Berlin, Germany

[3] Faculty of Natural Sciences, Institute of Chemistry, Materials for Innovative Energy Concepts, Technische Universität Chemnitz, 09107 Chemnitz, Germany

[*] Corresponding author: E-mail address: marc.armbruester@chemie.tu-chemnitz.de (M. Armbrüster)

Abstract

The intermetallic compound $InPd_2$ was prepared as single-phase material and used in an unsupported state as catalyst in the semi-hydrogenation of ethyne in a large excess of ethene. $InPd_2$ showed high activity and selectivity (up to 93%) towards ethene in the temperature range from 478 to 508 K. In addition, the compound revealed high stability during 20 h time on stream at 473 K at 80% selectivity and >90% conversion. Investigations by differential thermal analysis combined with thermogravimetry (DTA/TG) in H_2 and near-ambient pressure X-ray photoelectron spectroscopy (NAP-XPS) exclude the formation of intermetallic hydrides, phase transitions, decomposition, and the presence of elemental palladium. The stability of $InPd_2$ under reaction conditions allows addressing the influence of electronic factors on the catalytic properties by comparison to Ga-Pd intermetallic compounds. From the joint results of experiments and first-principles calculations, the electronic influence on the catalytic selectivity is found to be minor; selectivity seems to be largely governed by geometric effects – as suggested earlier by the site-isolation concept – as well as the absence of hydridic hydrogen.

Keywords

Pd_2In, Pd-Ga, Pd_2Ga, PdGa, intermetallic compound, electronic structure, *in situ* stability, XPS, DTA/TG, semi-hydrogenation, ethyne

Introduction

Intermetallic compounds as model catalysts allow studying structural and electronic influences on heterogeneously catalyzed reactions. A prerequisite is the stability of the compounds under reaction conditions, which ensures the presence of the pre-selected structural and electronic characteristics of the catalytic material. Having studied structural influences on the selectivity in the semi-hydrogenation of ethyne by utilizing the site-isolation concept with different, but structurally well-ordered Ga-Pd compounds,[1-3] the question on the electronic influence on the selectivity in this reaction remains open. The electronic factor can be addressed by investigating the intrinsic catalytic properties of isostructural intermetallic compounds. This minimizes local structural differences between two compounds, enabling to study electronic influences on the catalytic properties.

Among the intermetallic Ga-Pd compounds, $GaPd_2$ possesses high selectivity and excellent activity in the industrially important semi-hydrogenation of ethyne towards ethene, representing an essential cleaning step in the synthesis of polyethene.[4-6] The semi-hydrogenation reduces the concentration of ethyne in the ethene feed to the low ppm range, which otherwise poses a threat for the polymerization catalyst.[7] The intermetallic compound $InPd_2$ is isostructural to $GaPd_2$[8] (Co_2Si type of crystal structure) making it an excellent candidate to explore electronic influences on the catalytic properties. Being isostructural is a necessary, but not sufficient criterion. In addition, the *in situ* stability has to be investigated to ensure the presence of the pre-selected crystal and electronic structure of the compound under reaction conditions. Since some intermetallic compounds are prone to the formation of intermetallic hydrides,[9] the possible absorption of hydrogen needs special attention. A first study on the bulk hydride formation behavior of $InPd_2$ using *in situ* differential scanning calorimetry resulted in negligible hydrogen uptake even at pressures of up to 39 MPa.[10]

To enhance the knowledge about the stability in catalytically relevant atmospheres, differential thermal analysis combined with thermogravimetry (DTA/TG) in hydrogen atmosphere is employed as a sensitive tool to detect the mass change and the thermal signals accompanying bulk hydride formation. Since heterogeneous catalysis takes place on the surface of the material, near ambient pressure X-ray photoelectron spectroscopy (NAP-XPS) can be used to detect changes in the near-surface region and to determine the surface composition.[11]

Here the catalytic properties of the unsupported intermetallic compound $InPd_2$ in the semi-hydrogenation of ethyne in the presence of a large excess of ethene are presented and compared to the ones of GaPd as well as $GaPd_2$. The *in situ* stability of $InPd_2$ was investigated using DTA/TG in hydrogen atmosphere and NAP-XPS measurements in the mbar range including depth profiling to detect changes in the subsurface region. The electronic structure was additionally studied by quantum chemical DFT calculations.

Experimental

Sample preparation

The intermetallic compound $InPd_2$ was prepared using elemental indium (foil, ChemPur, 99.99%) and palladium (granules, ChemPur, 99.95%) as starting materials. The elements were weighted in a 1:2 molar ratio in air and subsequently transferred into a glove box filled with argon (O_2 and H_2O < 1 ppm). The physical mixture was placed in a glassy carbon crucible and slowly heated in a high-frequency induction furnace (Hüttinger TIG 5/300). After the exothermic reaction of the elements the melt was annealed for 10 min at 1373 K before the oven was switched off, allowing the samples to cool to ambient temperature. To reach thermodynamic equilibrium, the samples were enclosed in evacuated quartz glass ampoules and annealed at 973 K for two weeks. Subsequently, the ampoules were quenched in water.

Powder X-ray diffraction and metallographic investigations

Samples for powder X-ray diffraction experiments were finely crushed in an agate mortar, re-annealed at 973 K for 24 h in evacuated quartz glass ampoules, and spread on a 6 µm thick Mylar® foil coated with vaseline. Measurements were conducted in transmission mode on a Guinier camera (Huber G670, image plate, Cu$K\alpha_1$, λ = 1.540562 Å, quartz monochromator). Samples were further characterized metallographically. After embedding the samples in epoxy resin and subsequent polishing, they were studied by optical as well as electron microscopy (JEOL 6610, W-cathode). Wavelength dispersive X-ray spectroscopy (WDXS) was conducted on a SX100 (Cameca).

Catalytic measurements

Prior to the catalytic measurements the samples were crushed in air and sieved to obtain a sieve-fraction between 80 and 100 µm. Based on the crystallographic density of 12.02 g*cm^{-}

^{3}, an average diameter of 90 µm and assuming a spherical particle shape, a specific surface area of 5.6×10^{-3} m^2*g^{-1} results. The $InPd_2$ powder was mixed with 150 mg catalytically inert BN (Aldrich, hexagonal, 99.5%, 325 mesh) to improve the flow characteristics of the reactants and the heat distribution in the catalyst bed. Measurements were conducted in a catalytically inert quartz glass reactor (inner diameter 7 mm) with a quartz glass frit to support the catalyst bed. A total flow of 30 cm^3*min^{-1} consisting of 0.5 vol.% C_2H_2 (Praxair, pre-mixed 5% C_2H_2 (99.6%) in He (99.996%)), 5 vol.% H_2 (Praxair, 99.999%), 50 vol.% C_2H_4 (Westfalen Gas, 99.95%) in He (Praxair, 99.999%) was used for temperature-dependent (298 K to 688 K, 19.0 mg $InPd_2$) and isothermal (473 K, 28.5 mg $InPd_2$) measurements. Gases were mixed using mass flow controllers (Bronkhorst) and the gas phase composition was analyzed using a gas chromatograph (Varian Micro GC CP4900) using three different columns (molecular sieve, Al_2O_3 and polydimethylsiloxane). Conversion X of ethyne and selectivity S towards ethene were calculated as

$$X_{C_2H_2} = \frac{c_{in}-c_{out}}{c_{in}} \times 100\% \text{ and}$$

$$S_{C_2H_4} = \frac{(c_{C_2H_2,in}-c_{C_2H_2,out})}{(c_{C_2H_2,in}-c_{C_2H_2,out}) + c_{C_2H_6,out} + 2c_{C_4H_x,out}} \times 100\%.$$

Here, c_{in} represents the ethyne concentration in the feed and c_{out} is the ethyne concentration in the outlet gas. Due to the high ethene concentration in the feed, small changes in its concentration caused by the hydrogenation of ethyne can not be detected. Therefore, it is assumed that ethyne is only hydrogenated to ethene, which may be further hydrogenated to ethane. Higher hydrocarbons with more than four carbon atoms were not observed in the experiments.

Thermal analysis

Differential thermal analysis (DTA) and thermogravimetric (TG) measurements were simultaneously conducted on a Netzsch STA 449 F3 DTA/TG equipped with a gas mixing unit to supply a 25% H_2 (Praxair, 99.999%) in He (Praxair, 99.999%) atmosphere. 161.15 mg of sample in an alumina crucible were employed at a total flow of 12 cm^3*min^{-1} and a heating rate of 5 $K*min^{-1}$ from 298 K to 773 K. The empty alumina crucible was used for background correction by blind measurements.

X-ray photoelectron spectroscopy

X-ray photoelectron spectroscopy (XPS) was conducted using synchrotron radiation at beamline ISISS-PGM at the Helmholtz Zentrum Berlin für Materialien und Energie – Electron storage ring BESSY II. A detailed description of the set-up can be found elsewhere.[11] For the measurements, dense pills of $InPd_2$ (8 mm in diameter, 1 mm thick) were pressed from finely ground powder in stainless steel pressing tools. XP spectra were measured in HV ($p < 10^{-8}$ mbar) and under near-ambient pressure. Such an *operando* experiment included introduction of the gases at room temperature (90 vol.% H_2 and 10 vol.% ethyne, 1 mbar of total pressure), equilibration of the gas atmosphere for 15 min and subsequently heating the sample to 473 K with 20 $K*min^{-1}$. After equilibration for 15 min, the XP spectra were recorded. The binding energy scale of each spectrum was calibrated by recording the Fermi edge at the respective photon energy. By varying the energy of the incoming radiation, the spectral shape of Pd3*d* and In3*d* and the elemental composition was assessed for various information depths. Spectra were evaluated using Casa XPS.[12] Fitting parameters are listed in Table 1.

For quantitative analysis, the intensity of the signals was corrected for differences in ring current and photon flux before applying tabulated cross sections[13] to calculate elemental ratios. Determination of the information depth is based on the calculation of the inelastic mean free path (IMFP) using the NIST Electron IMFP Database.[14] The information depth is three times the IMFP, thus 95% of all excited electrons originate from the respective depth.[15] The thickness of surface layers was calculated according to ref. [16]. To verify the catalytic activity during the *operando* measurements, gas-phase analysis was carried out using a Balzers quadrupole mass spectrometer connected by a leak valve to the experimental cell.

Quantum Chemical Calculations

First-principles electronic structure calculations were conducted within the local density approximation (LDA) of the density functional theory (DFT) using the version 9.01 of the all-electron, full-potential local-orbital (FPLO®) package.[17] Exchange-correlation effects were considered by employing the Perdew-Wang parametrization.[18] The semi-core and valence states are treated at the scalar-relativistic level. Lower-lying core states are treated fully relativistic. A well-converged grid of 20×24×18 (20×22×18) containing 1430 (1320) irreducible *k*-points was used to sample the Brillouin zone of $InPd_2$ ($GaPd_2$). For elemental Pd and the intermetallic compound GaPd a 20×20×20 *k*-point grid containing 256 and 700

irreducible points was applied, respectively. The atom-centered charge densities were expanded up to l_{max} = 12. Electronic structure calculations of the intermetallic compound $InPd_2$ are based on the reported experimental lattice parameters of the present study, while calculations of elemental Pd (Cu type of crystal structure), GaPd and $GaPd_2$ are based on lattice parameters and atomic coordinates from Refs. [8;19;20]. To calculate the atomic charges in $InPd_2$, the electron density was derived from calculations using the tight-binding linear-muffin-tin-orbital (TB-LMTO) program in the atomic sphere approximation (ASA),[21] which was subsequently integrated and assigned to basins using the version 4.6 of the program DGrid,[22] a procedure based on the quantum theory of atoms in molecules (QTAIM) proposed by Bader.[23] Since it was not possible to reach total space filling of the unit cell volume using moderate overlap values, it was necessary to introduce small empty spheres, resulting in total space filling with an acceptable atom-atom overlap of 14%. The following radii of the atomic spheres were applied for $InPd_2$: *r*(In) = 1.65 Å, *r*(Pd1) = 1.42 Å, *r*(Pd2) = 1.47 Å. The radii of the empty spheres were in the range of 0.37-0.58 Å.

Results and Discussion

The intermetallic compound $InPd_2$ is obtained by melting the elements in the required ratio by induction heating and subsequent annealing at 973 K for two weeks. The samples are brittle and can be crushed in an agate mortar. Characterization by powder X-ray diffraction (Figure 1) shows that all diffraction peaks can be assigned to the intermetallic compound $InPd_2$ (space group *Pnma*, *a* = 5.6149(6) Å, *b* = 4.2160(6) Å, *c* = 8.226(1) Å, Co_2Si type of structure[24]) and is, together with the results from metallography, confirming the single-phase nature of the sample.

The crystal structure of $InPd_2$ comprises two different crystallographic palladium positions, each with a coordination of thirteen atoms (Fig. 1). Out of these, eight nearest neighbors are palladium atoms. The closest Pd-Pd distance in $GaPd_2$ is 2.8165 Å,[8] while the closest Pd-Pd distance in $InPd_2$ (2.8497 Å) is only marginally longer by 1.2%. In both compounds the number of Pd-Pd contacts is significantly lower than in elemental palladium (12 Pd neighbors) and the distance between the palladium atoms (2.7511 Å for elemental palladium)[20] is increased by around 4%. These structural features result in a nearly identical site-isolation for both compounds, making them valuable candidates to test for electronic

influences in the semi-hydrogenation of ethyne. In contrast, the main group elements in the Co_2Si type of structure are surrounded by ten transition metal atoms. As opposed to the closest Pd-Pd distance, which varies by only 1.2% between $GaPd_2$ and $InPd_2$, the closest distances between palladium and the main group metal are 2.5438 Å and 2.6891 Å for $GaPd_2$ and $InPd_2$, respectively, corresponding to a difference of 5.7%. Since the isolation of the transition metal atoms is likely to be decisive for the selectivity, the larger difference in the latter distances should be only of minor influence on the catalytic properties.

As mentioned above, exchanging gallium by indium is not causing major changes to the atomic arrangement within the crystal structure of $GaPd_2$. One would expect more important differences in their respective electronic structures. Valence band structures obtained from the calculated electronic density of states (DOS) and XPS experiments on as-prepared samples are compared in Figure 2. The experimental position as well as the width of the main valence band peak (photon energy of 720 eV and 770 eV for $InPd_2$ and $GaPd_2$, respectively) are in good agreement with the quantum chemical calculations, thus validating the bulk electronic structure as representation of the surface electronic structure in these cases. Especially the low density of states at the Fermi energy confirms the absence of elemental palladium, which would result in a large number of states at the Fermi energy.

As shown in Figure 3, $InPd_2$ and $GaPd_2$ display rather similar density of states. In both cases, the partial Pd4*d* DOS contributes the most to the total DOS just below the Fermi energy (E_F). They all exhibit a band-gap around -6 eV, and significantly modify the electronic structure near the Fermi level when compared to elemental Pd.[6;25] These strong modifications result from the formation of covalent bonds in the intermetallic compounds, which is indicated by the intermixing (hybridization) of the Pd4*d* and 4*s* states with the *s* and *p* valence electrons of the main group metals. As in many other intermetallic compounds, these features can be linked with a higher thermodynamic stability of $InPd_2$ and $GaPd_2$ in comparison to elemental Pd.[1;6;25;26] A detailed analysis of the chemical bonding applying the electron localizability approach[27] to both compounds is ongoing. Integration of the electron density obtained by the LMTO calculations resulted in a charge transfer from In to Pd ($In^{0.8+}Pd_2^{0.4-}$), which is in accordance to their respective Pauling electronegativities (In 1.8; Pd 2.2[28]).

Because of these similarities, it is necessary to quantify the differences between the intermetallic compounds $InPd_2$ and $GaPd_2$ to shed light on how dissimilar the electronic

structures are in contrast to the respective atomic structures.[29-32] Details of the Pd4*d* partial density of states (pDOS) of $InPd_2$ and $GaPd_2$ are shown in Table 2 together with the ones from the intermetallic compound GaPd (FeSi type of crystal structure) and elemental Pd (Cu type of crystal structure) (the Pd4*d* pDOS was convoluted with a Gaussian function (σ = 0.6 eV) and subsequently normalized to the maximum intensity for a straight forward comparison). $InPd_2$ and $GaPd_2$ hold small differences in their respective centers of gravity (0.3 eV) and *d*-band widths (0.4 eV) (Table 2). Furthermore, the obtained value of the density of states at the Fermi level is identical in both compounds. Hydride formation in these cases is excluded because PdH causes a narrowing of the Pd valence *d*-band together with a shift towards lower energies of the Pd DOS. Thus, states are depleted from the *d*-band region when Pd interacts with hydrogen. The bonding state between Pd and H forms a new band below the bottom of the Pd *d*-band and the Fermi energy is shifted upward relative to the *d*-band. This upward shift reduces the DOS at the Fermi level. These effects are also observed in Pd_4H, but to a less extent. [33]

In summary, the two compounds possess very similar electronic and atomic structures, thus the relative influence of these factors can not be set apart strictly and a simple relation between them and the catalytic properties observed in these compounds is difficult to obtain. On the other hand, GaPd and $GaPd_2$ present more noticeable differences in their respective electronic structures, despite their very similar catalytic semi-hydrogenation properties (in both cases selectivity to ethene is 75% [1;6]). Particularly, GaPd presents a much narrower *d*-band width (by 0.9 eV) as well as a lower DOS at the Fermi level (by 0.2 states*eV^{-1}*$atom^{-1}$) and a lower lying center of gravity (by 0.4 eV) than $GaPd_2$. Therefore, the observed catalytic performances of both compounds in the semi-hydrogenation of ethyne can be better associated with the active-site isolation concept, where both systems present similar geometrical features (Pd-Pd distances listed in Table 2). In the same line, we can anticipate that $InPd_2$ will perform similar to $GaPd_2$ in the semi-hydrogenation due to the isolation of the active sites. However, a small increase in selectivity might be expected because of its more specific (narrower) *d*-band[34;35] and the 1.2% increase in the closest Pd-Pd distance.

In situ stability

The correlation of the calculated electronic and structural characteristics with the catalytic properties is only possible if the compounds are stable under reaction conditions. While this has been proven for $GaPd_2$,[36] the *in situ* stability of $InPd_2$ has not yet been investigated. A

study by *Kohlmann* showed that $InPd_2$ is not absorbing significant amounts of hydrogen even at a pressure of 39 MPa.[10] This is valuable information, since intermetallic compounds can be prone to hydride formation, resulting in changes of the electronic as well as crystallographic structure. To study the temperature-dependent stability of $InPd_2$ under H_2 containing atmosphere, combined differential thermal analysis (DTA) and thermogravimetry (TG) at ambient pressure were employed. The obtained DTA and TG traces of $InPd_2$ in 25% H_2 in He from 298 K to 773 K are shown in Figure 4. Over the whole temperature range neither exothermic nor endothermic signals could be detected, indicating no phase transition, hydride formation nor decomposition of the compound. The TG measurement showed only a very small mass loss of 0.1% starting at 520 K. Since this temperature is too high for the desorption of adsorbed water, it is assigned to the reduction of oxidic species on the surface of the $InPd_2$ particles, due to the air contact of the sample.

After excluding bulk hydride formation, the near-surface region of bulk $InPd_2$ was investigated by XPS in high vacuum (HV) as well as under near-ambient pressure at one mbar pressure. The *operando* activity is confirmed by the observation of the mass traces of C_2H_4/C_2H_6 in the mass spectra (Figure 5). 15 minutes after reaching the steady state, XP spectra are recorded.

To determine possible compositional variations within the near-surface region as well as to test for modifications in the subsurface region, non-destructive depth-profiling was applied by variation of the energy of the incoming photons. In HV, $InPd_2$ is only showing one symmetric Pd3*d* signal at 335.4 eV (Fig. 6), which is shifted by 0.4 eV to higher binding energy compared to elemental palladium (335.0 eV[37]). The signal does not significantly change its position (i.e. >0.1 eV) with variation of the photon energy, only the FWHM is decreasing the more surface sensitive the measurements become. This observation is assigned to the decreasing resolution of the XPS measurements with increasing photon energy. The binding energy shift reveals the strong modification of the electronic structure of elemental palladium after the formation of $InPd_2$, exhibiting the same trend as observed for $GaPd_2$,[36] GaPd[25] and ZnPd.[38]

Concerning the In3*d* region, two signals are observed. The first corresponds to a binding energy of 443.4 eV, while the second is located at 444.4 eV (Figure 6). Comparison to literature data[39] and considering the weight loss detected in the DTA/TG measurements leads to the assignment of the signal at 444.4 eV to an oxidized In species. This leaves the

signal at 443.4 eV for the intermetallic indium in $InPd_2$, corresponding to a shift to lower binding energy of around 0.4 eV compared to elemental indium 443.84 eV.[40] The assignment of oxidized and intermetallic indium in the spectra is further corroborated by comparison of the variation of the intensity-ratio of the two signals with the incident photon energy. Increasing volume contribution leads to decreasing intensity of the signal at 444.4 eV, while the signal at 443.4 eV gains intensity. This is in line with either oxidized indium patches or a closed oxide layer on the surface. To distinguish between the two models, the thickness of the oxide layer was calculated based on the IMFP and the intermetallic/oxide ratio at three different depths, assuming a closed layer. As result, a thickness of 2 Å and 1 Å was obtained under HV and *in situ* conditions, respectively. This excludes a closed oxidic layer, showing the accessibility of the intermetallic surface, which is reflected in the significant catalytic activity of the sample right from the start (Fig. 5 and Fig. 7). By further analysis of the intermetallic contribution to the Pd3*d* and In3*d* spectra, the Pd:In ratio can be derived, revealing a surface which is slightly enriched in indium (Fig. 6c) which is very similar to $GaPd_2$, whose surface is enriched in gallium.[41;42] In both cases the enrichment is likely caused by the oxophilicity of the main group metal. Nevertheless, with increasing probing depth, the composition approaches the bulk composition of $In_{1.00(2)}Pd_{1.94(3)}$ as obtained by WDX.

Upon exposure of the sample to reaction conditions, no changes were observed in the case of the Pd3*d* spectra (Fig. 6a). In contrast, some changes occurred in the In3*d* region (Fig. 6b). In reductive atmosphere and at elevated temperature, most of the signal corresponding to oxidized indium is lost. Comparison of the intermetallic Pd:In ratio under reactive atmosphere to the one obtained in HV reveals a slight decrease, corresponding to the diffusion of the reduced indium into the intermetallic near-surface region. Thus, the near ambient pressure investigations reveal a high stability of the bulk and the surface of $InPd_2$ against hydride formation. In addition, no decomposition of the intermetallic compound was detected in the investigated temperature range. This surface stability also enables the bulk DOS being directly applied to study the catalytic properties as discussed above.

Catalytic properties

Even though the surface of $InPd_2$ is rich in indium, the experimental valence band structure of the surface corresponds well to the calculated valence band structure of the bulk. Having established the stability of $InPd_2$ under reaction conditions, the catalytic performance

of unsupported $InPd_2$ in the semi-hydrogenation of ethyne was measured in the presence of large amounts of ethene to mimic industrial conditions (C_2H_2:C_2H_4 = 1:100). Since the intermetallic surface is not fully covered with oxides, $InPd_2$ should be catalytically active. Temperature-dependent measurements reveal an activity maximum at 507 K (Fig. 7a). With up to 93% the selectivity towards ethene is very high up to 600 K and, interestingly, increases with increasing conversion in the temperature range from 425 – 575 K. The C4-selectivity of $InPd_2$ shows a peculiar behavior, being high at low and high temperature and showing a broad minimum at conversions higher than 10%. At temperatures higher than 600 K, the C4-fraction becomes the main product. The fully hydrogenated product ethane is only observed in relatively large amounts (up to 30%) below 450 K. Whereas the temperature-dependent experiment revealed the expected high selectivity towards ethene (Fig. 7a), the stability and deactivation behavior (e.g. by carbon deposits or sintering) should be assessed separately.

To allow direct comparison with the catalytic properties of the isostructural compound $GaPd_2$, $InPd_2$ was tested under identical conditions, i.e. isothermally at 473 K and conversions between 90-95%. Under these conditions, $InPd_2$ reveals a very high stability and an excellent selectivity of 80% towards ethene (Fig. 7b). In comparison to the selectivity of unsupported $GaPd_2$ of 75%, the selectivity of $InPd_2$ is slightly higher. This is in accordance with the expectations from the slightly larger Pd-Pd distance[43,44] as well as the quantum chemical calculations, from which a slightly higher selectivity for $InPd_2$ is expected because of the narrower *d* block in comparison to $GaPd_2$.[34;35]

Under reaction conditions, $InPd_2$ and $GaPd_2$ reveal a ratio of Pd:In or Pd:Ga in the near-surface region of 1.6 (Fig. 6 and Ref. [42]). Deriving the specific surface area by purely geometrical considerations (5.6×10^{-3} m^2g^{-1} for $InPd_2$ and 2.1×10^{-2} m^2g^{-1} for $GaPd_2$), a specific activity can be estimated by assuming that all Pd atoms in the near-surface region are catalytically active. With 31 and 29 molecules ethyne per Pd atom and per second the specific activities of $InPd_2$ and $GaPd_2$, respectively, are very similar. In contrast, the activity of unsupported GaPd is only 1/30 of $GaPd_2$.[42] This reveals a qualitative trend between the position of the *d* block and the specific activity for the intermetallic compounds: The closer the *d* block is to the Fermi energy, the higher the activity is. Puzzling is the rather low specific activity of elemental palladium (1-2 $mol_{C_2H_2}mol_{Pd}^{-1}s^{-1}$ [3][45]) which should be much higher due to the location of the *d* states. Considering the rich *in situ* sub-surface chemistry of palladium,[46] this can be rationalized. Upon formation of palladium hydrides, the band structure is only weakly affected in the vicinity of the Fermi energy,[47] thus a very active but

unselective catalytic behavior is expected ($W_d \approx 5$ eV, $G_c = -2.4$ eV). In contrast, calculations on hypothetical Pd carbides in the NiAs and the NaCl type of structures result in a strongly structured *d*-band with similar number of states at the Fermi level than elemental Pd (three sections, total $W_d \approx 5$ eV, $G_c = -3.1$ eV, $DOS(E_F) \approx 0.6$ states*eV^{-1}*$atom^{-1}$).[48] These changes are very similar to the ones occurring upon formation of the intermetallic compounds and might contribute to the higher selectivity of palladium catalysts when the subsurface Pd/C phase is present.[49] In addition, the experimentally observed stabilities under reaction conditions follow the sequence derived from the DOS at the Fermi energy. The higher the DOS at E_F, the lower the stability against segregation or hydride formation should be,[26] leading to the sequence GaPd > $InPd_2$ ≈ $GaPd_2$ > Pd. Indeed, GaPd shows much less segregation than $GaPd_2$ or $InPd_2$[25] and Pd tends to form palladium hydrides and to allow sub-surface chemistry[46] – both effects being not present in the case of the intermetallic compounds.

In summary, the intermetallic compound $InPd_2$ reveals a slight increase in selectivity compared to $GaPd_2$, which can be expected due to the small increase in the closest Pd-Pd distance as well as the narrower *d* block. This high selectivity leads to excellent long-term stability since deactivation by carbonaceous deposits is avoided. Surprisingly, the palladium atoms in $InPd_2$ and $GaPd_2$ are 30 times more active than in GaPd. The reason for this difference in specific activity is not known yet, but might be due to the differences in the electronic structures, i.e. the shift of the *d* block closer to the Fermi energy. The site-isolated intermetallic compounds $InPd_2$, $GaPd_2$ and GaPd – the latter possessing a very different electronic structure – reveal all very similar selectivities towards ethene in the semi-hydrogenation of ethyne. This is a strong indication that the atomic arrangement has an overwhelming effect on the selectivity in the semi-hydrogenation of ethyne. Catalytic investigations on other intermetallic compounds are ongoing to further investigate the different influences.

Conclusion

The intermetallic compound $InPd_2$ was successfully synthesized as single-phase material. Comparison of its crystal structure to isostructural $GaPd_2$ reveals only marginal structural differences between the two compounds. *Operando* measurements in reactive atmosphere

and in the presence of hydrogen confirmed the stability of $InPd_2$ and the absence of hydride formation and phase transitions.

Catalytic testing of $InPd_2$ in the semi-hydrogenation of ethyne revealed excellent stability and slightly higher selectivity to ethene of 80% than for $GaPd_2$ (75%). Comparison of the electronic structure of $InPd_2$ and $GaPd_2$ depict only small differences, which does not allow assigning the small selectivity differences to the electronic influences. Considering the catalytic behaviour and electronic structure of GaPd, a possible minor influence of the width of the Pd4*d* band on the catalytic selectivity is identified, while a position of the *d*-band closer to the Fermi energy seems to enhance the activity strongly. In conclusion, the selectivity towards ethene is governed mainly by the active-site isolation, verifying the site-isolation concept in ethyne semi-hydrogenation.

Acknowledgement

We thank the Helmholtz Zentrum Berlin für Materialien und Energie – Electron storage ring BESSY II for the provided beamtime at the ISISS-PGM beamline (Project No. 2009_1_80693) and H. Borrmann and U. Burkhardt for XRD measurements and metallography investigations, respectively. Insightful discussion with R. Schlögl is gratefully acknowledged.

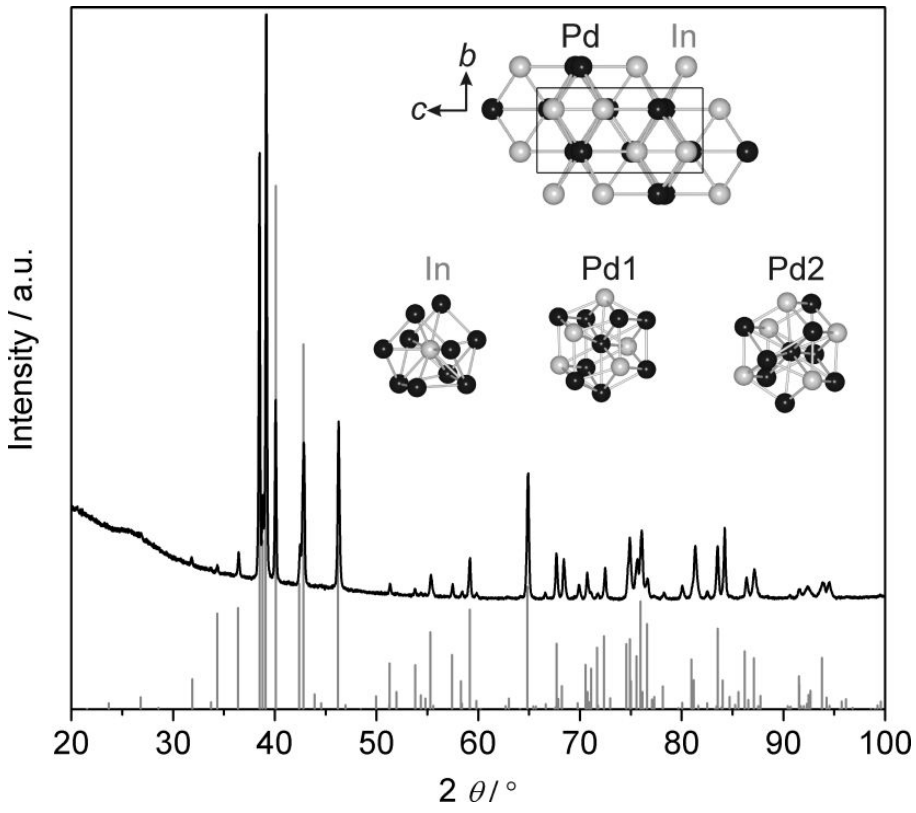

Figure 1: Powder X-ray diffraction pattern (top) and calculated diffraction pattern (bottom) of $InPd_2$. The insets display the crystal structure of $InPd_2$ and atomic environments of In, Pd_1 and Pd_2, respectively.

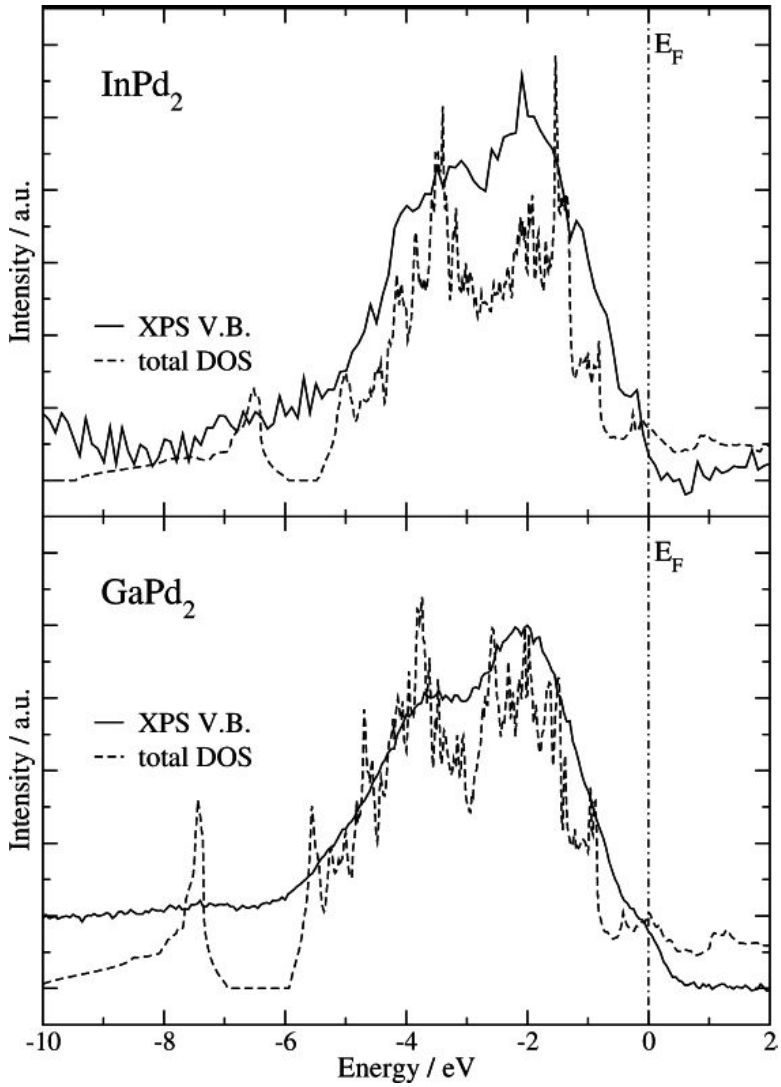

Figure 2: Comparison of experimental (obtained from XPS) and theoretical (obtained by DFT calculations) valence band structures of $InPd_2$ (top, photon energy 720 eV) and $GaPd_2$ (bottom, 770 eV) in the as-prepared state.

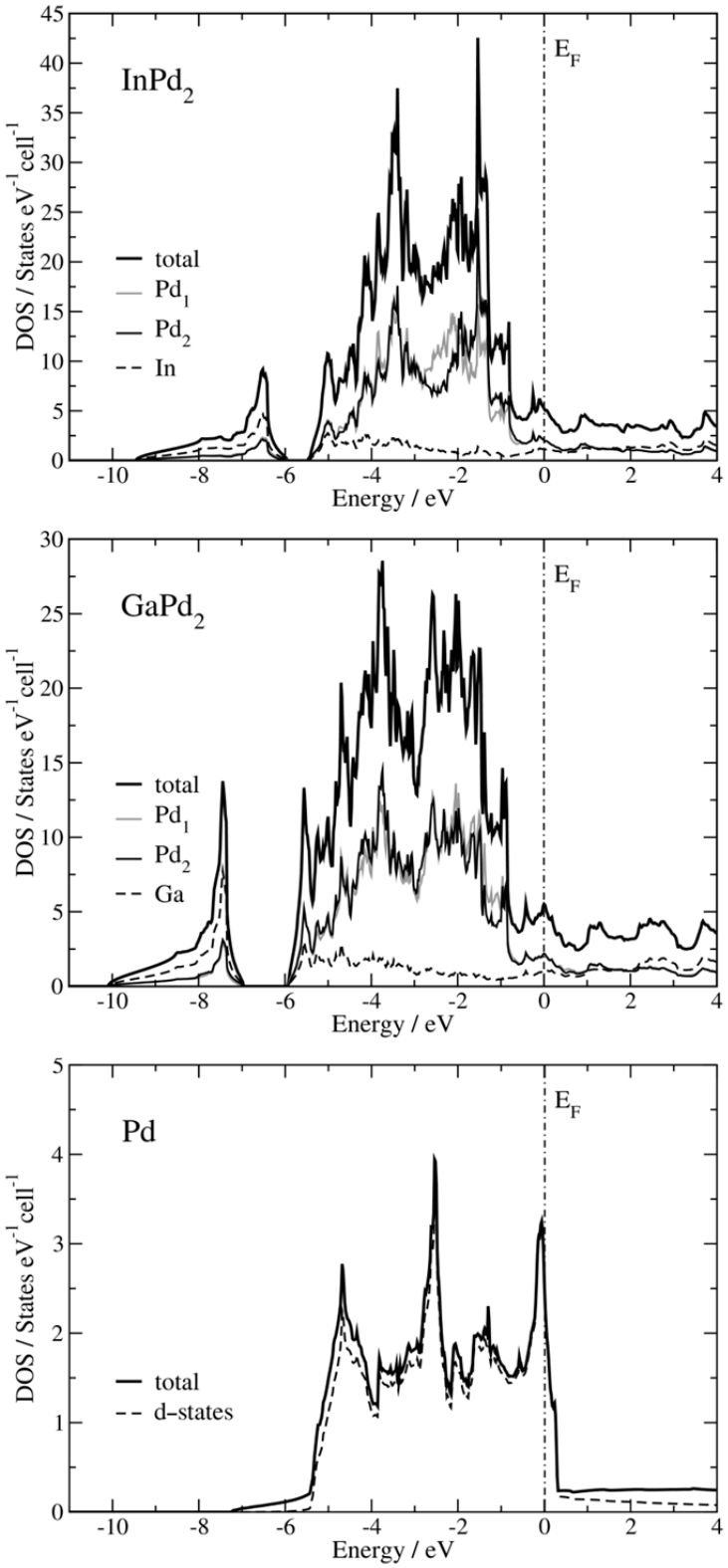

Figure 3: Added-up total and partial bulk density of states of $InPd_2$, $GaPd_2$ and elemental Pd.

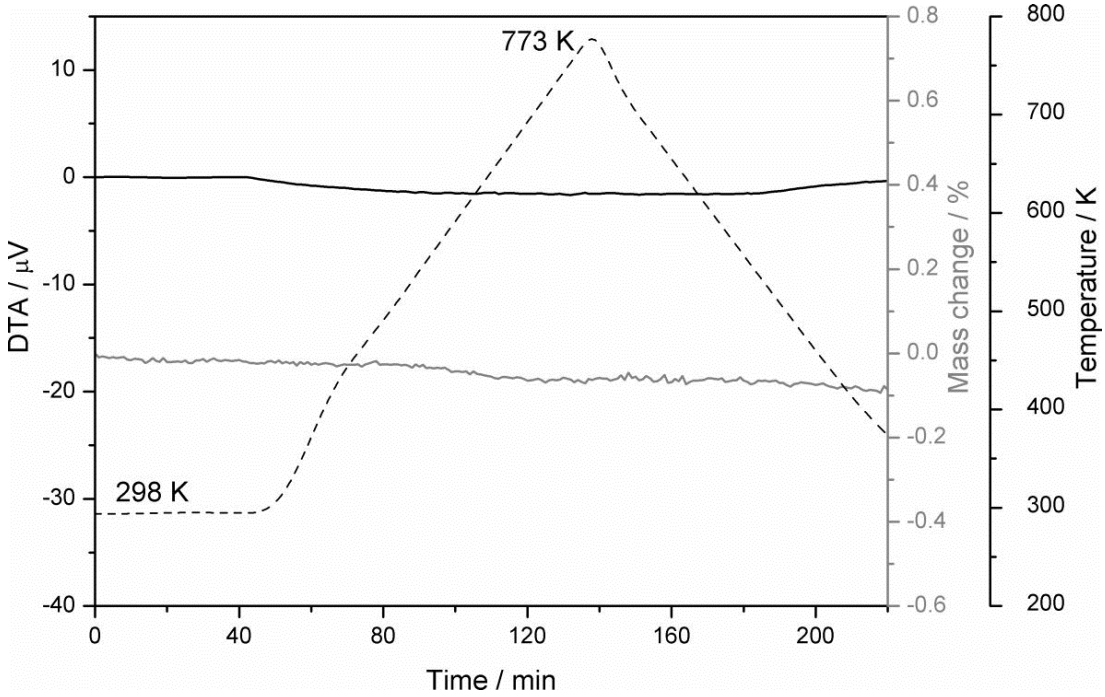

Figure 4: Temperature-programmed DTA/TG measurement of 161.15 mg $InPd_2$ in 25% H_2/He.

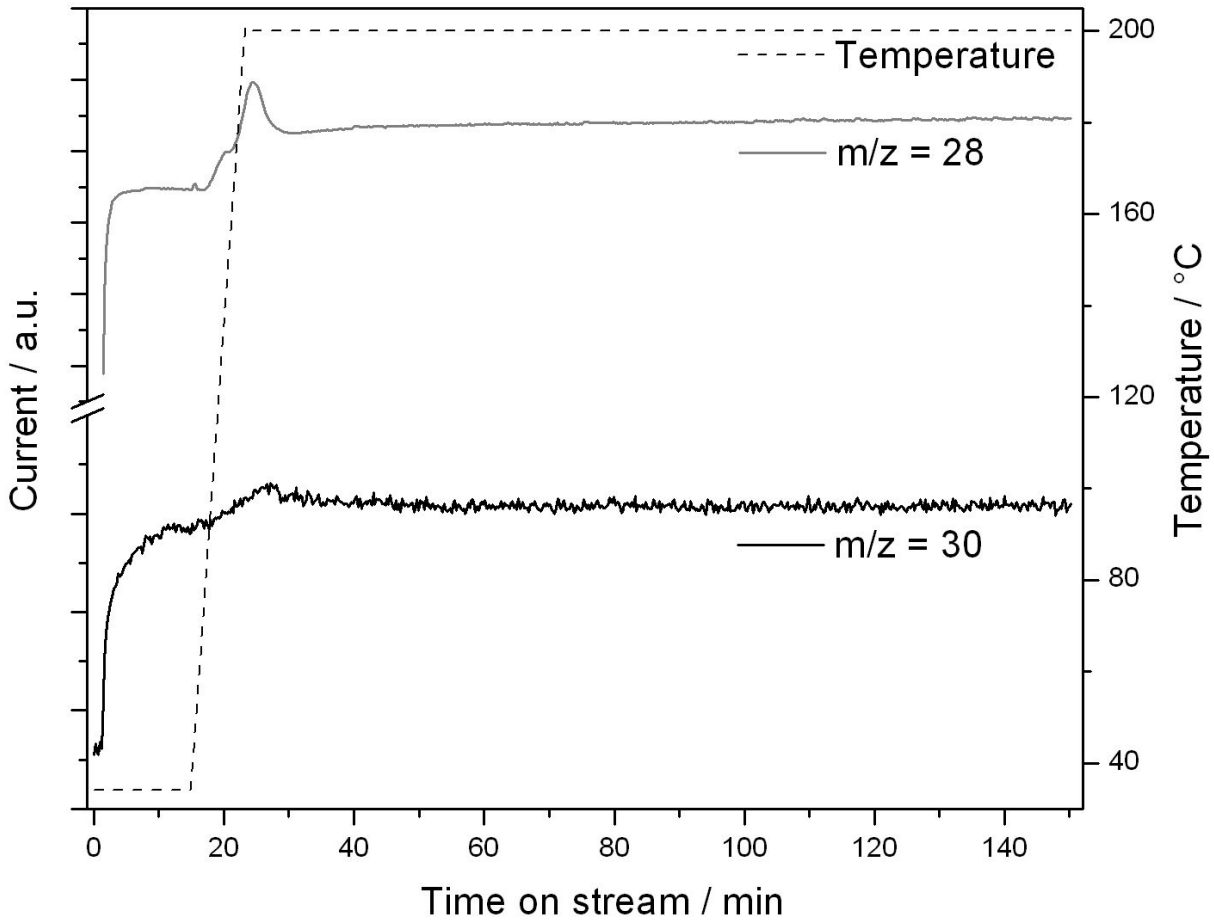

Figure 5: Mass spectrum of C_2H_4/C_2H_6 under *operando* XPS conditions ((90 vol.% H_2 and 10 vol.% C_2H_2, 1 mbar of total pressure).

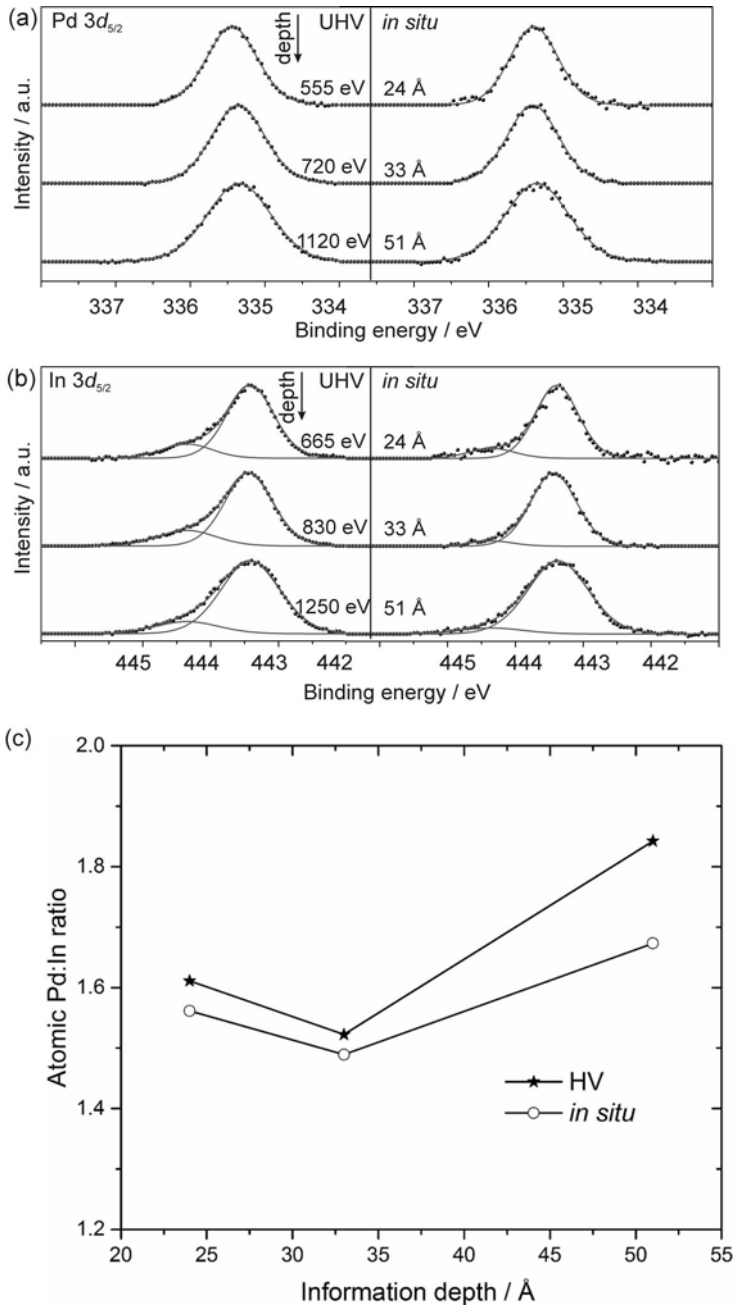

Figure 6: XP spectra of Pd $3d_{5/2}$ (a) and In $3d_{5/2}$ (b) region before (HV) and under *in situ* conditions at 473 K using different photon energies; Black full circles are the experimental results and grey lines represent the fit. The calculated information depths of the spectra (peak heights normalized) are also given. (c) atomic ratios of the intermetallic Pd and In species at different depths under HV and *in-situ* conditions (lines are a guide to the eye).

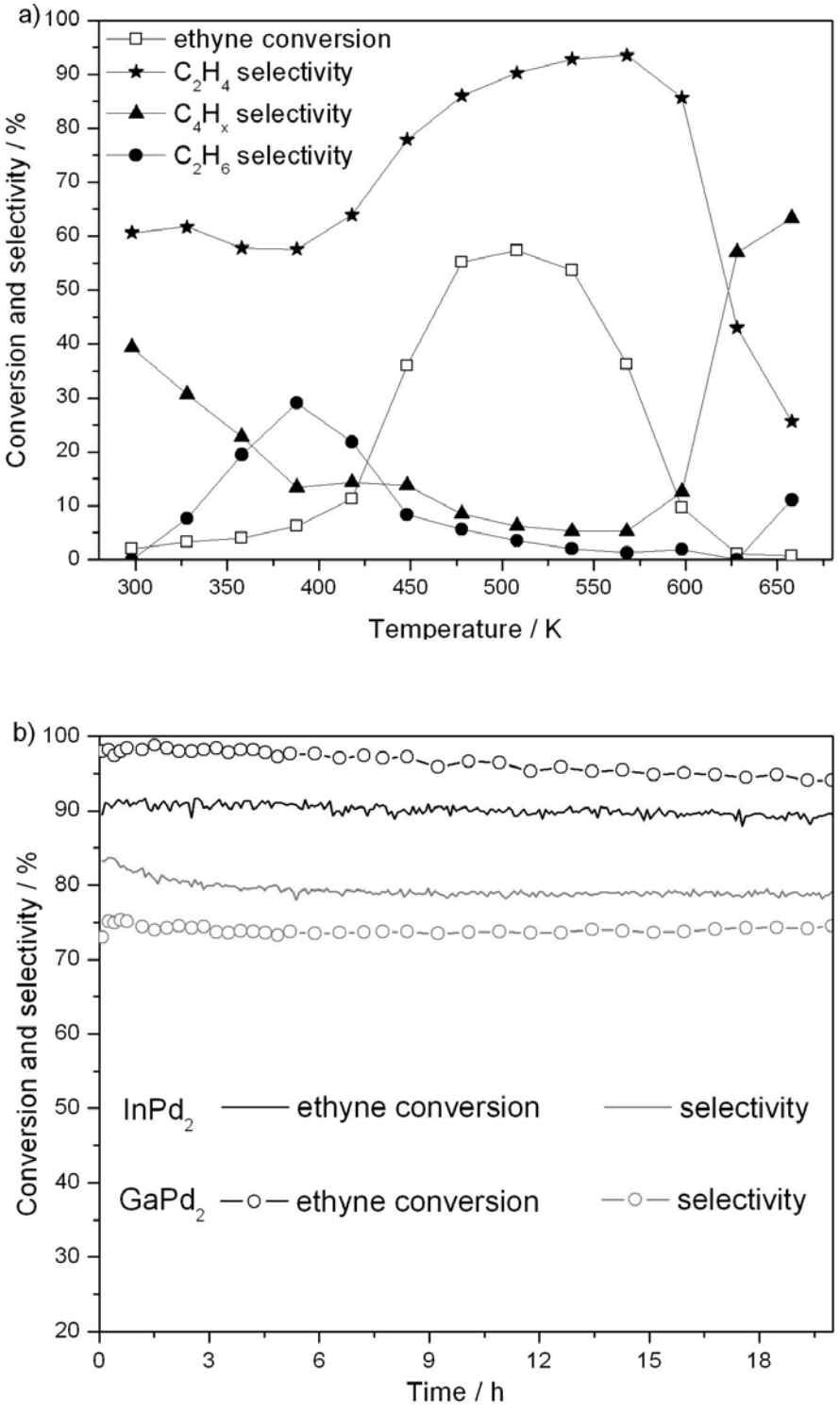

Figure 7: (a) Temperature-dependent conversion of ethyne and selectivity to ethene of $InPd_2$ (19 mg) in the semi-hydrogenation of ethyne; (b) isothermal measurement at 473 K of $InPd_2$ (28.5 mg) and $GaPd_2$ (10.0 mg). Gas-phase composition: 0.5% C_2H_2, 5% H_2, 50% C_2H_4 in He.

Table 1: XPS fitting parameters applied.

	$\mathbf{In_{oxidized}}$	$\mathbf{In_{intermetallic}}$	**Pd**
Peak position ($3d_{5/2}$)	444.4 eV	443.5 eV	335.5 eV
Peak shape	DS(0.01, 200)GL(80)	GL(30)	DS(0.05, 400)GL(99)
FWHM	0.9-1.2 eV	0.7-1.0 eV	0.74-1.0 eV

Table 2: Comparison of the closest Pd-Pd distance, the width of the Pd 4*d* block (W_d), its center of gravity (G_c) and the density of states at Fermi level (DOS(E_F)) as well as the specific activity and selectivity in semi-hydrogenation for $InPd_2$, $GaPd_2$, GaPd, and elemental Pd.

material	shortest Pd-Pd distance /Å	W_d /eV	G_c /eV	DOS(E_F) /states*eV^{-1} *atom^{-1}	A$^{\blacklozenge}$ /mol$_{C_2H_2}$mol$_{Pd}^{-1}$s^{-1}	S_{ethene} /%
$InPd_2$	2.8497	3.6	-2.6	0.3	31	79
$GaPd_2$	2.8165	4.0	-2.9	0.3	29	75
GaPd	3.0084	3.1	-3.3	0.1	1	75
Pd	2.7511	5.4	-2.4	0.6	1-2$^{\Delta}$	17$^{\Delta}$

$^{\blacklozenge}$ specific activity is determined by the amount of converted C_2H_2 per second over the active Pd in the near-surface region

$^{\Delta}$ data of 5 wt.-% Pd/Al_2O_3 from Ref. [3], calculation is based on the specific Pd-surface area of 5.6 m^2g^{-1}, and from review [43]

Reference List

[1.] M. Armbrüster, K. Kovnir, M. Behrens, D. Teschner, Yu. Grin, R. Schlögl, *J. Am. Chem. Soc.* **2010,** *132* 14745-14747.

[2.] J. Osswald, R. Giedigkeit, R. E. Jentoft, M. Armbrüster, F. Girgsdies, K. Kovnir, T. Ressler, Yu. Grin, R. Schlögl, *J. Catal.* **2008,** *258* 210-218.

[3.] J. Osswald, K. Kovnir, M. Armbrüster, R. Giedigkeit, R. E. Jentoft, U. Wild, Yu. Grin, R. Schlögl, *J. Catal.* **2008,** *258* 219-227.

[4.] A. Ota, M. Armbrüster, M. Behrens, D. Rosenthal, M. Friedrich, I. Kasatkin, F. Girgsdies, W. Zhang, R. Wagner, R. Schlögl, *J. Phys. Chem. C* **2011,** *115* 1368-1374.

[5.] A. Ota, J. Kröhnert, G. Weinberg, I. Kasatkin, E.L. Kunkes, D. Ferri, F. Girgsdies, N. Hamilton, M. Armbrüster, R. Schlögl, M. Behrens, *ACS Catal.* **2014,** *4* 2048-2059.

[6.] K. Kovnir, M. Armbrüster, D. Teschner, T. V. Venkov, F. C. Jentoft, A. Knop-Gericke, Yu. Grin, R. Schlögl, *Sci. Technol. Adv. Mater.* **2007,** *8* 420-427.

[7.] A. Borodzinski, G. C. Bond, *Catal. Rev. Sci. Engin.* **2006,** *48* 91-144.

[8.] K. Kovnir, M. Schmidt, C. Waurisch, M. Armbrüster, Yu. Prots, Yu. Grin, *Z. Kristallogr.- NCS* **2008,** *223* 7-8.

[9.] H. Kohlmann, in *Encyclopedia of Physical Science and Technology* ,*Vol. 9*, Academic Press, San Diego, CA **2002**, pp. 441-458.

[10.] H. Kohlmann, *J. Sol. State Chem.* **2010,** *183* 367-372.

[11.] A. Knop-Gericke, E. Kleimenov, M. Hävecker, R. Blume, D. Teschner, S. Zafeiratos, R. Schlögl, V. I. Bukhtiyarov, V. V. Kaichev, I. P. Prosvirin, A. I. Nizovskii, H. Bluhm, A. Barinov, P. Dudin, M. Kiskinova, Adv. Catal. **2009,** *52* 213-272.

[12.] Casa XPS, vers. 2.3.16, **2010**.

[13.] J. J. Yeh, I. Lindau, *Atomic Data and Nuclear Data Tables* **1985,** *32* 1-155.

[14.] C. J. Powell, A. Jablonski, *NIST Electron Inelastic-Mean-Free-Path Database - Version 1.2*, National Institute of Standards and Technology, Gaithersburg, MD **2010**.

[15.] J. C. Vickermann, I. Gilmore, *Surface Analysis: The Principal Techniques*, 2nd ed. John Wiley & Sons Ltd., Chichester **2009**.

[16.] H. Yamamoto, Y. Baba, T. A. Sasaki, *Surf. Sci.* **1996,** *349* L133-L137.

[17.] K. Koepernik, H. Eschrig, *Phys. Rev. B* **1999,** *59* 1743-1757.

[18.] J. P. Perdew, Y. Wang, *Phys. Rev. B* **1992,** *45* 13244-13249.

[19.] M. Armbrüster, H. Borrmann, M. Wedel, Yu. Prots, R. Giedigkeit, P. Gille, *Z.Kristallogr.- NCS* **2010,** *225* 617-618.

[20.] C. N. Rao, K. K. Rao, *Canadian J. Phys.* **1964,** *42* 1336-1342.

[21.] O. Jepsen, A. Burkhardt, O. K. Andersen, The Program TB-LMTO-ASA, vers. 4.7, **2000**, Max-Planck-Institut für Festkörperforschung, Stuttgart.

[22.] M. Kouhout, DGrid, vers. 4.6, **2012**, Max-Planck-Institut für Chemische Physik fester Stoffe, Dresden.

[23.] R. F. W. Bader, *Atoms in Molecules: A Quantum Theory*, Oxford University Press, Oxford **1990**.

[24.] H. Kohlmann, C. Ritter, *Z. Naturf. B* **2007,** *62* 929-934.

[25.] K. Kovnir, M. Armbrüster, D. Teschner, T. V. Venkov, L. Szentmiklósi, F. C. Jentoft, A. Knop-Gericke, Yu. Grin, R. Schlögl, *Surf. Sci.* **2009,** *603* 1784-1792.

[26.] E. Belin-Ferré, *Surface Properties and Engineering of Complex Intermetallics*, World Scientific, Singapore **2010**.

[27.] A. I. Baranov, M. Kohout, *J. Comp. Chem.* **2011,** *32* 2064-2076.

[28.] L. Pauling, *The Nature of the Chemical Bond and the Structure of Molecules and Crystals*, 3rd ed. Cornell University Press, Ithaca **1960**.

[29.] T. Bligaard, J. K. Nørskov, Electrochim. Acta **2007,** *52* 5512-5516.

[30.] J. K. Nørskov, T. Bligaard, B. Hvolbaek, F. Abild-Petersen, I. Chorkendorff, C. H. Christensen, *Chem.Soc.Rev.* **2008,** *37* 2163-2171.

[31.] M. Mavrikakis, B. Hammer, J. K. Nørskov, *Phys. Rev. Lett.* **1998,** *81* 2819-2822.

[32.] B. Hammer, J. K. Nørskov, Adv. Catal. **2000,** *45* 71-129.

[33.] C. T. Chan and S. G. Louie, Phys. Rev. B 1983, 27 3325-3337.

[34.] K. Nozawa, N. Endo, S. Kameoka, A. P. Tsai, K. Ishii, *J. Phys. Soc. Japan* **2011,** *80* 064801.

[35.] A. P. Tsai, S. Kameoka, Y. Ishii, *J. Phys. Soc. Japan* **2004,** *73* 3270-3273.

[36.] K. Kovnir, D. Teschner, M. Armbrüster, P. Schnörch, M. Hävecker, A. Knop-Gericke, Yu. Grin, R. Schlögl, *BESSY Highlights 2007* **2008,** 22-23.

[37.] D. Teschner, A. Pestryakov, E. Kleimenov, M. Hävecker, H. Bluhm, H. Sauer, A. Knop-Gericke, R. Schlögl, *J. Catal.* **2005,** *230* 186-194.

[38.] M. Friedrich, D. Teschner, A. Knop-Gericke, M. Armbrüster, *J. Catal.* **2012,** *285* 41-47.

[39.] M. Faur, M. Faur, D. T. Jayne, M. Goradia, C. Goradia, *Surf. Interf. Anal.* **1990,** *15* 641-650.

[40.] C. J. Powell, *J. Electron Spectrosc. Rel. Phenom.* **2012,** *185* 1-3.

[41.] G. Wowsnick, D. Teschner, I. Kasatkin, F. Girgsdies, M. Armbrüster, A. Zhang, Yu. Grin, R. Schlögl, M. Behrens, *J. Catal.* **2014**, *309* 209-220.

[42.] G. Wowsnick, D. Teschner, M. Armbrüster, I. Kasatkin, F. Girgsdies, R. Schlögl, M. Behrens, *J. Catal.* **2014,** *309* 221-230.

[43.] W. M. H. Sachtler, *Catal. Rev. Sci. Eng.* **1976** *14* 193-210.

[44.] M. Armbrüster, R. Schlögl, Yu. Grin, *Sci. Technol. Adv. Mater*. **2014**, *15* 034803.

[45.] A. Borodzinski, G. C. Bond, *Catal. Rev. Sci. Engin.* **2008**, *50* 379-469.

[46.] M. Armbrüster, M. Behrens, F. Cinquini, K. Föttinger, Yu. Grin, A. Haghofer, B. Klötzer, A. Knop-Gericke, H. Lorenz, A. Ota, S. Penner, J. Prinz, C. Rameshan, Z. Révay, D. Rosenthal, G. Rupprechter, P. Sautet, R. Schlögl, L. Shao, L. Szentmiklósi, D. Teschner, D. Torres, R. Wagner, R. Widmer, G. Wowsnick, *ChemCatChem* **2012,** *4* 1048-1063.

[47.] X. Cui, X. X. Liang, J. T. Wang, G. Z. Zhao, *Chin. Phys. B* **2011,** *20* 026201.

[48.] L. Li, *Mod. Phys. Lett. B* **2008,** *22* 2937-2944.

[49.] D. Teschner, J. Borsodi, A. Wootsch, Z. Révay, M. Hävecker, A. Knop-Gericke, S. D. Jackson, R. Schlögl, *Science* **2008,** *320* 86-89.